

Exploitation of structural and regulatory diversity in glutamate racemases

Tomas Lundqvist^{1*}, Stewart L. Fisher^{2*}, Gunther Kern², Rutger H. A. Folmer¹, Yafeng Xue¹, D. Trevor Newton², Thomas A. Keating², Richard A. Alm² & Boudewijn L. M. de Jonge²

Glutamate racemase is an enzyme essential to the bacterial cell wall biosynthesis pathway, and has therefore been considered as a target for antibacterial drug discovery. We characterized the glutamate racemases of several pathogenic bacteria using structural and biochemical approaches. Here we describe three distinct mechanisms of regulation for the family of glutamate racemases: allosteric activation by metabolic precursors, kinetic regulation through substrate inhibition, and D-glutamate recycling using a D-amino acid transaminase. In a search for selective inhibitors, we identified a series of uncompetitive inhibitors specifically targeting *Helicobacter pylori* glutamate racemase that bind to a cryptic allosteric site, and used these inhibitors to probe the mechanistic and dynamic features of the enzyme. These structural, kinetic and mutational studies provide insight into the physiological regulation of these essential enzymes and provide a basis for designing narrow-spectrum antimicrobial agents.

Peptidoglycan is an essential component of the bacterial cell wall that determines the cell morphology and protects the bacteria from osmotic rupture¹. A key building block for peptidoglycan in pathogenic bacteria is D-glutamate, which is produced from L-glutamate by glutamate racemase (MurI)^{2–5}. Both L- and D-glutamate are vital for the survival of bacteria, and regulation of their relative levels is critical because of the central role of L-glutamate in protein synthesis and metabolism⁶. A regulation mechanism for *Escherichia coli* MurI has been reported^{7,8}. We set out to determine whether these observations extend to other species, and assess this enzyme as a target for broad-spectrum or species-specific antibacterial therapy. Remarkably, we found differences in enzyme kinetics, structure, and inhibition characteristics among glutamate racemases isolated from key pathogens. The discovery of potent specific inhibitors of *Helicobacter pylori* that act through inhibition of MurI by a novel allosteric mechanism demonstrates the potential to exploit these differences to identify selective agents.

Biochemical and structural characterization

MurI enzymes, selected on primary sequence divergence (see Supplementary Fig. S1), revealed significant differences in biophysical properties and steady-state kinetics (Table 1). *E. coli* MurI is monomeric in solution and shows extremely low intrinsic activity in either direction (symmetrical kinetic profile), but catalytic turnover was upregulated over 1,000-fold by UDP-MurNAc-Ala, the product of the preceding enzyme in the peptidoglycan biosynthetic pathway (Table 1)^{7,8}. This activation has been proposed as a feedback regulation mechanism for generating sufficient levels of D-glutamate to support cell growth, while maintaining high levels of L-glutamate, a key metabolic intermediate^{7–9}. In contrast, *H. pylori* MurI forms a dimer, is unaffected by UDP-MurNAc-Ala and demonstrates a high degree of asymmetry in substrate processing with the Michaelis constant (K_M) for D-glutamate approximately tenfold lower than for L-glutamate, and severe substrate inhibition by D-glutamate alone (Table 1). This profile can be attributed to a slow isomerization

step in the catalytic cycle, where substrate inhibition arises through oversaturation¹⁰, resulting in the lowest catalytic turnover of the MurI proteins studied, while retaining a similar overall catalytic efficiency ($k_{cat}/K_M \approx 8.5 \times 10^5 \text{ M}^{-1} \text{ min}^{-1}$). Physiologically, the asymmetric profile and severe substrate inhibition by D-glutamate provide a different regulatory mechanism to control the D-glutamate levels in *H. pylori*, which are significantly lower than L-glutamate levels (this is true in *E. coli* as well¹¹; see Supplementary Methods).

MurI enzymes from the Gram-positive species *Staphylococcus aureus*, *Enterococcus faecalis* and *Enterococcus faecium* share similar biophysical and biochemical characteristics that are distinct from *E. coli* and *H. pylori* MurI. All form homodimers in solution, are unaffected by UDP-MurNAc-Ala, and exhibit high intrinsic catalytic turnover (Table 1). These enzymes display asymmetry in substrate preference with elevated L-glutamate K_M values, but did not exhibit the severe substrate inhibition by D-glutamate seen for *H. pylori* MurI. As a result, the catalytic activity of these enzymes is not strictly governed; this may be because Gram-positive organisms require more D-glutamate than Gram-negative species because they have a thicker peptidoglycan layer. In addition, some of these organisms contain a D-amino acid transaminase^{12,13} and because MurI was shown to be essential in Gram-positive pathogens^{14,15}, it is likely that the transaminase is used to salvage excess D-glutamate.





The different kinetic profiles exhibited across the species suggested fundamental structural differences and therefore the MurI enzymes were characterized using X-ray crystallography. Crystal structures were generated for each enzyme under similar, physiologically relevant conditions and almost all of these contained substrates in the active site at full occupancy (Table 1).

The crystal structures of the MurI monomers all shared a conserved topology and fold (see Supplementary Fig. S2) that is comprised of two domains that exhibit a pseudo-symmetry axis (shown for *H. pylori* MurI in Fig. 1a), consistent with the structure recently reported for *Bacillus subtilis* RacE (ref. 16). Catalysis takes place at the interface of the two domains, with each domain contributing

¹AstraZeneca Global Structural Chemistry, AstraZeneca R&D Mölndal, SE-431 83, Mölndal, Sweden. ²Infection Discovery, AstraZeneca R&D Boston, Waltham, 02451 Massachusetts, USA.

*These authors contributed equally to this work.

Table 1 | Biochemical and structural data of MurI proteins

MurI protein	Biochemical data			Structural data		
	$K_{M,L/D}$ (μM), $k_{\text{cat},L/D}$ (min^{-1}) and $K_{I_s,L/D}$ (μM)		UDP-MurNAC-Ala activation	Oligomerization state	Complex (resolution)	Schematic representation
<i>H. pylori</i>	$K_{M,L} = 740 \pm 50$ $k_{\text{cat},L} = 63 \pm 1$	$K_{M,D} = 63 \pm 0.4$ $k_{\text{cat},D} = 12 \pm 0.2$ $K_{I_s,D} = 5.8 \pm 0.03$	No	Dimer	D-glutamate (1.9 Å); see Fig. 1a D-glutamate + compound A (1.86 Å); see Fig. 3a	 Head-head dimer
<i>H. pylori</i> A75T	$K_{M,L} = 7,430 \pm 840$ $k_{\text{cat},L} = 107 \pm 4$	$K_{M,D} = 275 \pm 38$ $k_{\text{cat},D} = 3.9 \pm 0.3$ $K_{I_s,D} = 661 \pm 66$	No	Dimer		
<i>H. pylori</i> E151K	$K_{M,L} = 7,360 \pm 240$ $k_{\text{cat},L} = 136 \pm 2$	$K_{M,D} = 282 \pm 6$ $k_{\text{cat},D} = 5.0 \pm 0.03$ $K_{I_s,D} > 100,000$	No	Dimer		
<i>E. coli</i>	$K_{M,L} = 1,200 \pm 140^*$ $k_{\text{cat},L} = 730 \pm 20$	$K_{M,D} = 2,100 \pm 140$ $k_{\text{cat},D} = 2,600 \pm 44$	Yes	Monomer	L-glutamate + UDP-MurNAC-Ala (1.9 Å); see Fig. 1c	 Activator-modulated monomer
<i>E. faecalis</i>	$K_{M,L} = 1,200 \pm 12$ $k_{\text{cat},L} = 1,500 \pm 40$	$K_{M,D} = 250 \pm 20$ $k_{\text{cat},D} = 704 \pm 14$	No	Dimer	D-glutamate (1.95 Å)	 Tail-tail dimer
					D-glutamate + L-glutamate (2.5 Å); see Fig. 1d	 Mixed forms dimer
<i>E. faecium</i>	$K_{M,L} = 1,100 \pm 100$ $k_{\text{cat},L} = 2,200 \pm 50$	$K_{M,D} = 240 \pm 23$ $k_{\text{cat},D} = 900 \pm 32$	No	Dimer	Phosphate (1.8 Å)	Tail-tail dimer
<i>S. aureus</i>	$K_{M,L} = 4,600 \pm 270$ $k_{\text{cat},L} = 510 \pm 90$	$K_{M,D} = 140 \pm 10$ $k_{\text{cat},D} = 34 \pm 3$	No	Dimer	D-glutamate (2.15 Å)	Tail-tail dimer

The solution oligomerization state was determined using equilibrium analytical ultracentrifugation methods at concentrations ranging from 5 to 50 μM protein. Additional structural information is available in the Supplementary Methods and Tables. Data represent the mean \pm s.d. from nonlinear regressions fitting to the data ($n \geq 10$ velocity data points) using the Michaelis–Menten equation or the substrate-inhibition model equation. K_{I_s} is the substrate inhibition constant (see Supplementary Methods).

* The data for *E. coli* MurI were obtained in the presence of 400 μM UDP-MurNAC-Ala (fully activated).

the residues attributed to the enantiomeric deprotonations¹⁷. The domain that begins with the amino terminus (domain A) contains the conserved amino acids involved in deprotonation of D-glutamate (D7, S8, C70, T72), whereas the carboxy-terminal domain (domain B) contains the catalytic residues involved in L-glutamate deprotonation (E150, C181, T182, H183) (see Supplementary Fig. S3). Using domain A as an anchor, it is possible to overlay the monomers from the MurI structures. From this alignment, it is apparent that the two domains move with respect to each other and this movement is largely restricted to a rotation around a single axis, as illustrated for the *E. faecalis* structures (Fig. 1b). This hinge movement occurs at the two crossovers between the domains (rotation at a conserved glycine—G91 for the *H. pylori* structure—and kinking of a helix mainly mapping into domain A) and a coordinated hinge movement is required to form the active site and permit catalysis.

The observed hinge movement of MurI is not only critical for catalytic function, but also adapts activity to meet physiological demands. The three distinct regulatory mechanisms that were differentiated by biochemical studies can be rationalized through detailed analyses of the MurI structures. *E. coli* MurI co-crystallized as a monomer with both L-glutamate and its activator UDP-MurNAC-Ala. The activator binds in the hinge region on the side opposite to the catalytically active site (Fig. 1c) through contacts between the uracil ring system and domain B and through specific salt bridge interactions with R104 in domain A and the alanyl moiety of the activator (see Supplementary Fig. S4), consistent with the strict requirement of the alanine and uracil moieties for activation⁷. These interactions are predicted to focus the hinge movement and to favour productive substrate binding, leading to higher catalytic efficiency in response to cellwall biosynthesis demand.

In contrast, *S. aureus*, *E. faecalis* and *E. faecium* all form homodimeric structures (exemplified by *E. faecalis* in Fig. 1d), similar to that observed for *B. subtilis* RacE (ref. 16) and consistent with solution studies on these enzymes (Table 1). In all these structures, the

monomers oligomerize in a tail-to-tail orientation with active sites opposed and fully exposed to solvent. Oligomerization occurs through interactions across a C2 symmetry axis, mainly involving helices from the A and B domains of each monomer, to create an interface that is conserved in all of the Gram-positive MurI proteins structurally characterized so far. The flexibility of this interaction is nicely illustrated in the *E. faecalis* structure containing L- and D-glutamate, providing some insight into the conformational changes required for catalysis (Fig. 1b). An even wider range of hinge movements could be observed in *E. faecium* enzyme while it interacts with various salts, indicating that the hinge movement adapts to molecules binding in the active site (see Supplementary Methods). In contrast to the Gram-positive MurI structures, the *H. pylori* MurI enzyme also forms a homodimer but with the active sites in close proximity in a face-to-face orientation, shielded from the solvent (Fig. 1a) in a manner that is distinct from, but similar to, the structure of *Aquifex pyrophilus* MurI (ref. 18).

A similar interaction is observed in the asymmetric unit of the structure reported for *B. subtilis*; however, significant differences exist between the *H. pylori* and the *B. subtilis* structures in this dimer interface (see Supplementary Table S9 and Figs S11–S14), which indicates that whereas the *H. pylori* dimer interface is biologically relevant, the *B. subtilis* AB interface probably results from crystal packing interactions, as noted in ref. 16. To ensure that this dimer interface was not just a crystal packing interaction, two independent structure determinations of the native *H. pylori* enzyme were carried out using crystals grown under different crystallization conditions and crystallographic space groups (see Supplementary Table S4). Comparative analysis of these two crystals forms demonstrated that the dimer interface was fully conserved, but each crystal form had its own unique set of packing interactions. No other dimer interactions were observed in any of the investigated crystal forms.

The *H. pylori* MurI structure contained only D-glutamate in the active site, despite growing the crystals in the presence of saturating

concentrations of racemic glutamate. This finding is consistent with the asymmetric, D-glutamate-inhibited kinetic profile of the enzyme and the structure most probably represents the substrate-inhibited, resting state of the enzyme. This arrangement suggests that the enzyme has evolved to stabilize the closed, glutamate-bound state to reduce overall catalytic turnover. Although dimerization occurs through inter-monomer interactions between both A and B domains, the B-domain interactions possess the majority of dimerization contacts. Logically, during hinge-movement transition between closed and open states, it is the A-domain interface that is predicted to separate to allow glutamate to enter and leave, whereas the B-domain interface is maintained. This hypothesis is supported by analysis of the nuclear magnetic resonance (NMR) titrations with glutamate, which indicate that domain A is more dynamic (see Supplementary Figs S6–S8).

Selective inhibition mechanism

The structural and biochemical data clearly demonstrate distinguishing features among the MurI isozymes, and we envisioned that these differences could be exploited to identify selective inhibitors of *H. pylori* MurI. A high-throughput screen against the AstraZeneca compound collection (385,861 compounds) identified a pyrazolo-pyrimidinedione analogue (compound A; see structure in Fig. 2a) among the hit clusters. We chose compound A for further study because it had excellent potential for structural diversification. This compound demonstrated inhibition of the isolated enzyme and the enzyme in intact *H. pylori* cells (see Supplementary Methods), along

with excellent selectivity for *H. pylori* MurI. Inhibition by compound A had the hallmarks of stoichiometric, specific inhibition^{19,20}: it was time-independent, fully reversible and insensitive to changes in enzyme or detergent concentration. The lack of structural similarity to glutamate prompted a detailed biochemical analysis of the mode of inhibition. Remarkably, kinetic inhibition studies indicated that compound A does not compete with glutamate and that glutamate binding was required for inhibition (Fig. 2b).

This uncompetitive inhibition mechanism is exceedingly rare for single-substrate enzymes²¹. Despite this precedent, all of the biochemically confirmed hits from the screen had this mode of inhibition (about ten series); no inhibitors were identified that were competitive with the substrate. Protein NMR using ²H and ¹⁵N isotopically labelled *H. pylori* MurI was carried out, and in the absence of glutamate, two-dimensional transverse relaxation-optimized spectroscopy (TROSY) indicated that the protein was quite flexible, assuming multiple conformations. However, addition of glutamate generated a highly resolved NMR spectrum and allowed full backbone resonance assignments (Fig. 2c, see Supplementary Methods and Figs S6–S8). Subsequent addition of compound A to the substrate-saturated enzyme caused significant peak shifts, indicating compound binding (Fig. 2c). In contrast, adding compound A to the substrate-free enzyme had no marked effect on its poorly resolved spectrum, indicating that compound A binds preferably to the substrate-bound form of the enzyme. These results were further supported by direct binding measurements using isothermal titration

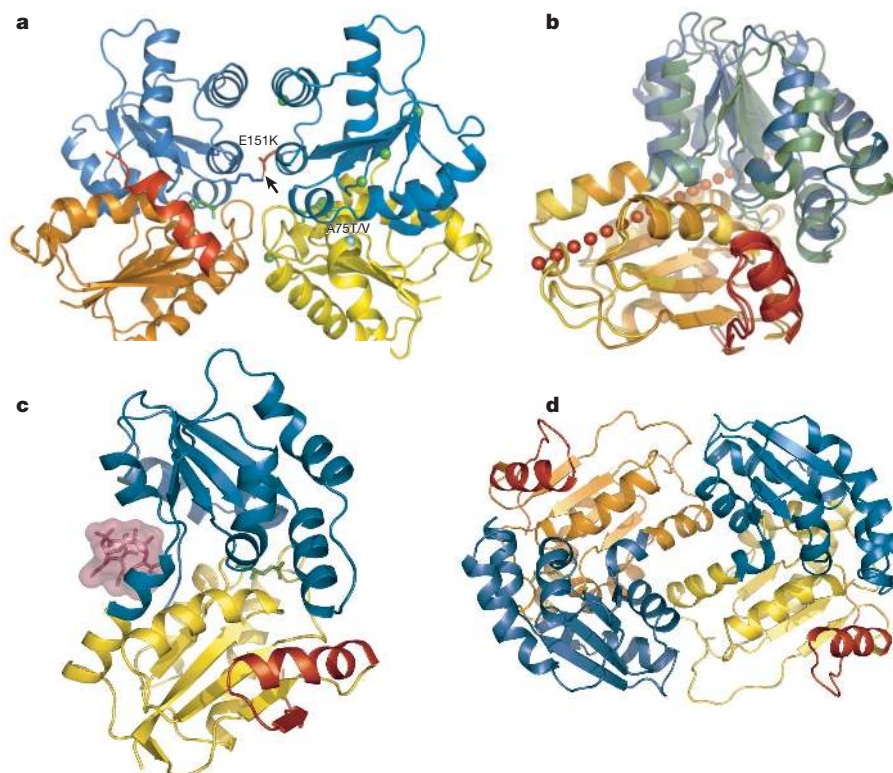


Figure 1 | Crystal structures of MurI proteins. **a**, Crystal structure of *H. pylori* MurI dimer containing D-glutamate (green) with monomer domains A (N-terminal domain; yellow/orange) and B (C-terminal domain; blue) and the C-terminal helix (red) in the left monomer highlighted. Resistance mutation sites A75T/V (cyan), E151K (red), A35T, C162Y, I178T, G180S, L186F, L206P, Q248R (all in green) and a putative intermonomer salt bridge contact between E151 & K117⁷ (arrow) are shown. **b**, Overlay of MurI monomers (based on domain A) from *E. faecalis*/L-glutamate (blue) and *E. faecalis*/D-glutamate (green). Domain A is indicated in light colours. Glutamate substrates are shown. The hinge axis is shown as a line of red spheres. **c**, Crystal structure of *E. coli* MurI containing L-glutamate (green)

and the activator UDP-MurNac-Ala (pink, $2F_o - F_c$ electron density map contoured at 1σ) with monomer domains A (yellow) and B (blue). The C-terminal helix and the 12-amino-acid C-terminal extension (relative to *H. pylori* sequence) are in red. The orientation is equivalent to the left monomer of *H. pylori* MurI in **a**. **d**, Crystal structure of *E. faecalis* MurI containing L- (right monomer) and D-glutamate (left monomer), showing monomer domains A (yellow/orange) and B (blue); the C-terminal helix and extension (relative to *H. pylori* sequence) are highlighted in red. The orientation of the right monomer is equivalent to the left monomer in *H. pylori* MurI in **a**.

calorimetry and by protein fluorescence quenching on compound titration, for which in each case saturating levels of glutamate were required for compound binding (see Supplementary Methods and Fig. S5).

Crystals of *H. pylori* MurI containing D-glutamate and compound A were produced and a high-resolution structure was solved for this enzyme–substrate–inhibitor complex. The inhibitor bound in a cryptic pocket formed by a dislocation of the C-terminal helix (Fig. 3a). To our knowledge, this is the only example of an uncompetitive inhibitor of a single-substrate enzyme in which the inhibitor binds at a cryptic allosteric site²², and it highlights the power of

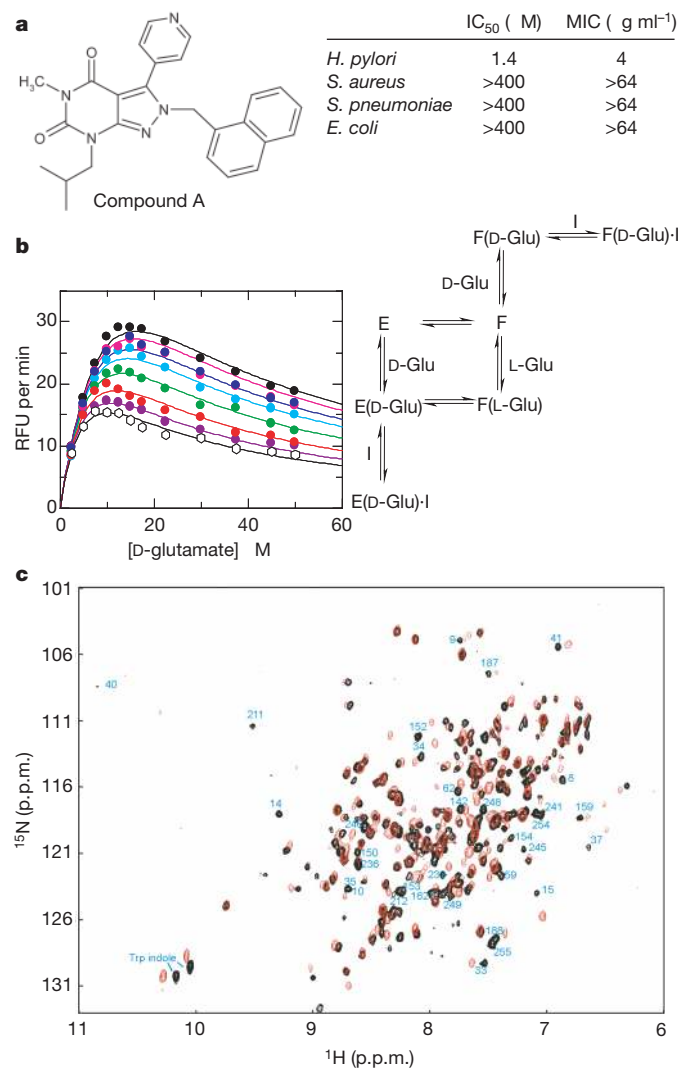


Figure 2 | Inhibitor characterization. **a**, Structure of the pyrazolopyrimidinedione inhibitor with *in vitro* activities. IC₅₀, half-maximal inhibitory concentration. MIC, minimal inhibitory concentration to prevent bacterial growth. **b**, Kinetic mechanism of inhibition data and scheme for *H. pylori* MurI. Kinetic data of enzymatic turnover inhibition were collected, simultaneously varying D-glutamate (2.5–50 μM) and compound A (0 μM (black symbols) to 3.5 μM (white open symbols), serial dilutions), and globally fitted to several models incorporating substrate inhibition. The best fit was found for the scheme shown, with inhibitor (I) binding to both the productive enzyme:substrate complex (E(D-Glu)) and the substrate-inhibited form of the enzyme (F(D-Glu)). RFU, relative fluorescence units. **c**, Two-dimensional TROSY ¹H, ¹⁵N NMR spectrum of 0.3 mM *H. pylori* MurI with 1.8 mM D-glutamate (black) and with 1.8 mM D-glutamate and 0.4 mM compound A (red). Spectral differences indicate compound binding. Backbone peak assignments to selected amino acids are indicated by residue primary sequence number. Tryptophan indole ring resonances are denoted for clarity.

high-throughput screening to find enzyme inhibitors serendipitously. As in other examples of allosteric inhibitor binding^{23–26}, the enzyme–substrate–inhibitor structure is highly similar to the native structure, with minimal differences from the native structure for regions outside the compound-binding site (root-mean-square deviation 0.718 Å for 488 Cα atoms in the dimer). However, in contrast to the precedents of allosteric inhibition, in which inhibitor binding initiates a cascade of residue movements that alters the active site, no changes were observed in the *H. pylori* MurI active site on inhibitor binding.

Comparison of the enzyme–substrate–inhibitor and native *H. pylori* MurI structures demonstrated that the inhibitor-binding site does not exist in the native structure because it is fully occupied by residues of the C-terminal helix (Fig. 3b), and formation of this site could not be predicted from the native structure by computational

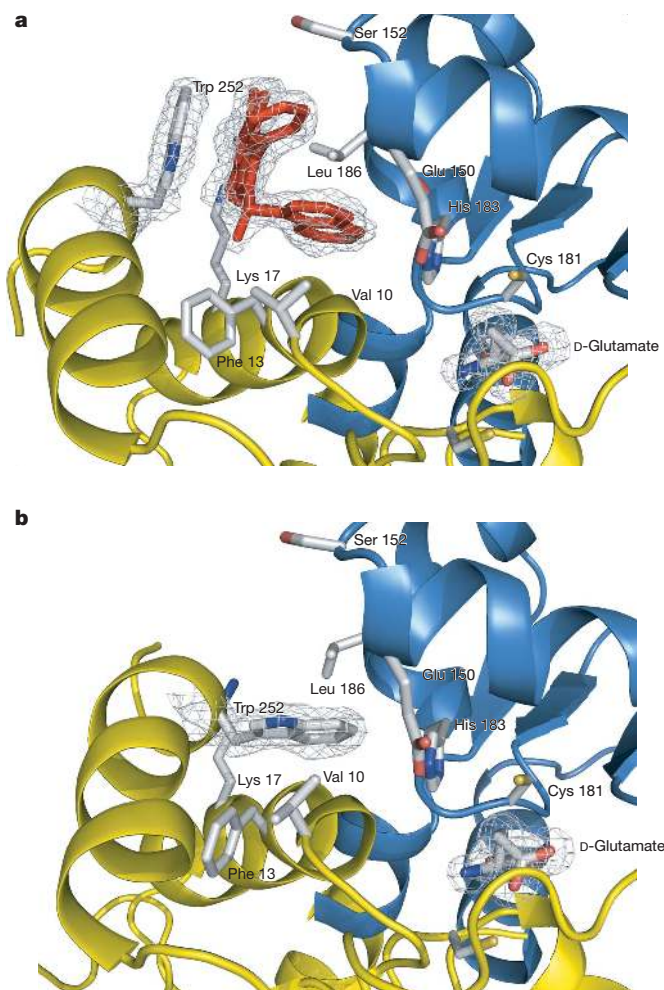


Figure 3 | Inhibitor-binding site in *H. pylori* MurI. **a**, Detailed view of compound binding site of the enzyme–substrate–inhibitor complex of *H. pylori* MurI and compound A. On compound binding, the C-terminal helix movement induces W252 side-chain displacement and rotation to form a surface for π-stacking with the pyrazolopyrimidinedione core of the inhibitor. The pocket vacated by the indole ring movement is filled with the naphthyl moiety of compound A and further stabilized by interactions with V10, G11 (not shown), H183, L186, and W244 (not shown). Additional interactions are formed between the isobutyl substituent of compound A and the F13, S14 (not shown), K17, L253 (not shown) residues, while the pyridyl ring substituent makes contacts with the main-chain atoms of residues E150 and S152. The N-methyl substituent resides in a large cleft that is accessible to solvent. Electron density map for compound A, the substrate and W244 are shown (2F_o–F_c electron density map contoured at 1σ) **b**, Detailed view of compound binding site in the native *H. pylori* MurI structure. Colour scheme and key residues annotated as described for Fig. 1a.

methods. For example, none of the residues affected by compound binding adopted unfavourable dihedral angles (considered markers of allosteric sites) in the native enzyme structure²². On compound binding, the C-terminal helix movement induces W252 side-chain displacement and rotation to form a surface for π -stacking with the pyrazolopyrimidinedione core of the inhibitor. The pocket vacated by the movement of the indole ring is filled with the naphthyl moiety of compound A and further stabilized by additional interactions (Fig. 3a). The crystal structure is consistent with the solution NMR analyses as the inhibitor-binding site residues exhibited strong spectral shifts on compound titration (see Supplementary Methods). Taken together, these data suggest that the compound binds to a conformation that is dependent on the substrate-bound state and results in further stabilization of a closed form of the enzyme, which precludes movement of the A domains to expose the active site and allow release of product.

A comparison of the *H. pylori* structure bound with compound A and other MurI structures revealed the basis for selectivity. In *E. coli* many of the key residues in the corresponding pyrazolopyrimidinedione-binding region of the *H. pylori* enzyme, which is distinct from the UDP-MurNAc-Ala-binding and active sites, are not conserved, including the critical W252 (see Supplementary Fig. S9). Further, the *E. coli* C-terminal helix has a 12-residue extension that folds back and forms part of the β -sheet core of domain A (Fig. 1c). This extension presumably restricts movement of the C-terminal helix and prevents pocket formation. Inspection of the corresponding inhibitor-binding regions of the Gram-positive MurI structures revealed significant variation in geometries, even though many of the binding site residues were conserved (see Supplementary Fig. S9). In addition, like the *E. coli* structure, all of these structures contain a C-terminal extension that forms additional interactions with the core of domain A; these interactions are likely to restrict movement of the C-terminal helix that is required for inhibitor binding site formation (Fig. 1d).

Potential resistance mechanism

Sequence analyses of diverse, clinically relevant *H. pylori* isolates showed that almost all of the interacting residues in this binding pocket were conserved in this species (see Supplementary Fig. S10), demonstrating the suitability of the site for inhibition of *H. pylori* MurI and indicating the importance of maintaining these residues. To assess the mutability of the binding pocket, an inhibitor with optimized potency was used to obtain resistant mutants (see Supplementary Methods). Mutants were not easily obtained because resistance rates using single-step selection methods were low.

The sequence analyses of those mutants that were obtained demonstrated that single amino acid changes distributed throughout the primary sequence of MurI generated the resistant phenotype. Only one of the mutations (L186F) was found in the inhibitor-binding pocket, indicating that mutations in this binding site are not well tolerated. The immutability of the allosteric compound-binding pocket is probably due to the critical role this site has in the hinge movement of the enzyme. All other mutations were located either at the dimer or domain interfaces, or within the core of domain B (Fig. 1a). In an effort to deconvolute the mechanism of resistance, two resistant mutant proteins, A75T and E151K, were purified and biochemically characterized.

Despite the fact that these mutations are not located within the active site of the enzyme, dramatic effects were observed in the kinetic profiles (Table 1). In both cases, increased substrate K_M values were observed along with compensatory changes in k_{cat} and the severe D-glutamate substrate inhibition observed with wild-type MurI was significantly reduced or absent. Further, the resistant mutant proteins had lower melting temperatures relative to the wild-type protein in the absence of substrate, but equivalent thermal stability in the presence of saturating substrate (see Supplementary Methods). These changes in kinetic and biophysical profile are expected to reduce the overall population of substrate-bound form of the enzyme under

physiological conditions, and thus the population of MurI to which these uncompetitive inhibitors bind (Fig. 2b). Although it is difficult to provide an easily validated structural rationalization for the A75T mutant, E151 does form an inter-monomer salt-bridge interaction with K117 in the native enzyme structure (Fig. 1a). This salt-bridge interaction helps stabilize the closed, substrate-bound form of the enzyme and the E151K mutation results in a repulsive interaction that disfavours substrate binding. Despite these changes, saturation of the enzyme *in vitro* with substrate overcomes this resistance mechanism, and the wild-type inhibitor affinity that was observed under saturating substrate conditions is consistent with this (see Supplementary Methods). The reduction of substrate-bound enzyme populations by decreasing substrate affinity while maintaining activity is a logical and ingenious solution to overcoming an uncompetitive inhibitor.

Prospects for inhibitor development

These structural, biophysical and enzyme kinetic studies have identified at least three distinguishable types of MurI: (1) monomeric enzymes modulated by allosteric activation by metabolic precursors; (2) head-to-head dimers regulated through substrate inhibition; and (3) tail-to-tail dimers with high intrinsic turnover that rely on D-glutamate recycling using a D-amino-acid transaminase for cellular glutamate pool-level regulation. The pyrazolopyrimidinedione series faces several further hurdles in the progression to clinical treatment of *H. pylori* infections, particularly in the areas of serum protein binding and metabolism, but nevertheless this series demonstrates the potential to exploit the differences across MurI proteins to discover selective inhibitors with potent cellular activity.

METHODS

See Supplementary Information for experimental details.

Enzyme preparation and biochemical characterization. Full-length MurI proteins were prepared by expression either as native (*H. pylori*, *E. coli*) or N-terminal 6His-tagged (*S. aureus*, *E. faecalis*, *E. faecium*) recombinant proteins in *E. coli* strains co-expressing the chaperone proteins GroEL/GroES²⁷ and purified using standard chromatographic methods. Enzyme activity was assayed by measuring the conversion of glutamate from D- to L-enantiomer using a coupled assay system monitoring the reduction of NAD⁺ to NADH by L-glutamate dehydrogenase. MurI activity in the L-to-D direction was coupled to MurD (UDP-MurNAc-Ala:D-glutamate ligase) and measured as a function of phosphate production using 2-amino-6-mercapto-7-methylpurine ribonucleoside and purine nucleoside phosphorylase (see Supplementary Methods). The protein oligomeric state was assessed using size exclusion chromatography with multi-angle light scattering detection and equilibrium or velocity sedimentation on a Beckman Optima XL-I Analytical ultracentrifuge over a range of enzyme concentrations.

Structural and conformational studies. Details on the crystallization conditions and refinement statistics for all protein structures can be found in Supplementary Tables S3–S8. NMR experiments were performed on *H. pylori* MurI (0.3 mM, pH 7.5) at 303 K on a Bruker Avance 800 MHz system, equipped with a triple-resonance (¹H/¹³C/¹⁵N) single-gradient 5 mm probe. Details of the procedures used for backbone assignments can be found in the Supplementary Methods. [¹⁵N, ¹H] correlation experiments were recorded to assess protein stability with increasing D-glutamate concentration and to map the binding site of compound A. Residues with sufficient resolution for mapping exhibiting backbone trace resonance shifts of two or more linewidths were considered significant.

Received 4 April 2006; accepted 14 February 2007.

- van Heijenoort, J. Recent advances in the formation of the bacterial peptidoglycan monomer unit. *Nat. Prod. Rep.* **18**, 503–519 (2001).
- Tanner, M. E. & Miao, S. The synthesis and stability of aziridino-glutamate, an irreversible inhibitor of glutamate racemase. *Tetrahedr. Lett.* **35**, 4073–4076 (1994).
- Ashiuuchi, M., Yoshimura, T., Esaki, N., Ueno, H. & Soda, K. Inactivation of glutamate racemase of *Pediococcus pentosaceus* with L-serine O-sulfate. *Biosci. Biotechnol. Biochem.* **57**, 1978–1979 (1993).
- de Dios, A. *et al.* 4-Substituted D-glutamic acid analogues: The first potent inhibitors of glutamate racemase (MurI) enzyme with antibacterial activity. *J. Med. Chem.* **45**, 4559–4570 (2002).

5. Glavas, S. & Tanner, M. E. The inhibition of glutamate racemase by D-N-hydroxyglutamate. *Bioorg. Med. Chem. Lett.* **7**, 2265–2270 (1997).
6. Newsholme, P., Procopio, J., Lima, M. M. R., Pithon-Curi, T. C. & Curi, R. Glutamine and glutamate—their central role in cell metabolism and function. *Cell Biochem. Funct.* **21**, 1–9 (2003).
7. Doublet, P., van Heijenoort, J. & Mengin-Lecreux, D. The glutamate racemase activity from *Escherichia coli* is regulated by peptidoglycan precursor UDP-N-acetylmuramoyl-L-alanine. *Biochemistry* **33**, 5285–5290 (1994).
8. Ho, H.-T. et al. UDP-N-acetylmuramyl-L-alanine functions as an activator in the regulation of the *Escherichia coli* glutamate racemase activity. *Biochemistry* **34**, 2464–2470 (1995).
9. Doublet, P., van Heijenoort, J. & Mengin-Lecreux, D. Regulation of the glutamate racemase of *Escherichia coli* investigated by site-directed mutagenesis. *Microb. Drug Resist. Mechanisms Epidemiol. Dis.* **2**, 43–49 (1996).
10. Fisher, L. M., Albery, W. J. & Knowles, J. R. Energetics of proline racemase: racemization of unlabeled proline in the unsaturated, saturated, and oversaturated regimes. *Biochemistry* **25**, 2529–2537 (1986).
11. Mengin-Lecreux, D., Flouret, B. & van Heijenoort, J. Cytoplasmic steps of peptidoglycan synthesis in *Escherichia coli*. *J. Bacteriol.* **151**, 1109–1117 (1982).
12. Fotheringham, I. G., Bledig, S. A. & Taylor, P. P. Characterization of the genes encoding D-amino acid transaminase and glutamate racemase, two D-glutamate biosynthetic enzymes of *Bacillus sphaericus* ATCC 10208. *J. Bacteriol.* **180**, 4319–4323 (1998).
13. Pucci, M. J., Thanassi, J. A., Ho, H. T., Falk, P. J. & Dougherty, T. J. *Staphylococcus haemolyticus* contains two D-glutamic acid biosynthetic activities, a glutamate racemase and a D-amino acid transaminase. *J. Bacteriol.* **177**, 336–342 (1995).
14. Song, J. H. et al. Identification of essential genes in *Streptococcus pneumoniae* by allelic replacement mutagenesis. *Mol. Cells* **19**, 365–374 (2005).
15. Wang, L. & Zamudio, C. A method for predicting operons in prokaryotes. US patent number US2005/0026189A1 (2005).
16. Ruzhenikov, S. N. et al. Substrate-induced conformational changes in *Bacillus subtilis* glutamate racemase and their implications for drug discovery. *Structure* **13**, 1707–1713 (2005).
17. Glavas, S. & Tanner, M. E. Active site residues of glutamate racemase. *Biochemistry* **40**, 6199–6204 (2001).
18. Hwang, K. Y. et al. Structure and mechanism of glutamate racemase from *Aquifex pyrophilus*. *Nature Struct. Biol.* **6**, 422–426 (1999).
19. McGovern, S. L., Helfand, B. T., Feng, B. & Shoichet, B. K. A specific mechanism of nonspecific inhibition. *J. Med. Chem.* **46**, 4265–4272 (2003).
20. Seidler, J., McGovern, S. L., Doman, T. N. & Shoichet, B. K. Identification and prediction of promiscuous aggregating inhibitors among known drugs. *J. Med. Chem.* **46**, 4477–4486 (2003).
21. Ghosh, N. K. & Fishman, W. H. On the mechanism of inhibition of intestinal alkaline phosphatase by L-phenylalanine. *J. Biol. Chem.* **241**, 2516–2522 (1966).
22. Hardy, J. A. & Wells, J. A. Searching for new allosteric sites in enzymes. *Curr. Opin. Struct. Biol.* **14**, 706–715 (2004).
23. Wiesmann, C. et al. Allosteric inhibition of protein tyrosine phosphatase 1B. *Nature Struct. Mol. Biol.* **11**, 730–737 (2004).
24. Pargellis, C. et al. Inhibition of p38 MAP kinase by utilizing a novel allosteric binding site. *Nature Struct. Biol.* **9**, 268–272 (2002).
25. Oikonomakos, N. G., Skamnaki, V. T., Tsitsanou, K. E., Gavalas, N. G. & Johnson, L. N. A new allosteric site in glycogen phosphorylase b as a target for drug interactions. *Struct. Fold. Des.* **8**, 575–584 (2000).
26. Hardy, J. A., Lam, J., Nguyen, J. T., O'Brien, T. & Wells, J. A. Discovery of an allosteric site in the caspases. *Proc. Natl Acad. Sci. USA* **101**, 12461–12466 (2004).
27. Anderson, M. et al. Crystals of Murl from Gram negative, Gram positive, and atypical bacterium; computer-assisted method for screening, identifying, and designing inhibitors of Murl; inhibitors of Murl; and uses thereof. US patent number US2005/0037478 A1 (2005).

Supplementary Information is linked to the online version of the paper at www.nature.com/nature.

Acknowledgements We thank M. Gowravaram for compound synthesis and characterization, and all members of the Murl Team and collaborators across AstraZeneca for support of this work.

Author Contributions S.L.F. and T.L. contributed equally to this work. S.L.F., G.K., D.T.N. and T.A.K. performed the protein biochemical and kinetic characterizations, Y.X. solved the *H. pylori* Murl Native I structure and T.L. solved all other protein structures. R.H.A.F. performed the NMR studies, R.A.A. performed the phylogenetic, genomic and sequence analyses and B.L.M.d.J. performed the microbial physiology analyses. All authors discussed the results, contributed and commented on the manuscript.

Author Information The atomic coordinates of the protein structures have been deposited in the European Bioinformatics Institute Macromolecular Structure Database: *H. pylori* Murl complexed with D-glutamate (Native I, accession code 2jfx; Native II, accession code 2jfy); *H. pylori* complex with D-glutamate and compound A, accession code 2jgz; *E. coli* Murl complexed with L-glutamate and UDP-MurNAc-Ala, accession code 2jfn; *S. aureus* Murl complexed with D-glutamate, accession code 2jfq; *E. faecalis* Murl complexed with D- or L-glutamate, accession code 2jfo; *E. faecalis* Murl complexed with D-glutamate, accession code 2jfp; *E. faecium* Murl complexed with phosphate, accession code 2jfu; *E. faecium* Murl complexed with citrate, accession code 2jfv; *E. faecium* Murl complexed with tartrate, accession code 2jfw. Reprints and permissions information is available at www.nature.com/reprints. The authors declare no competing financial interests. Correspondence and requests for materials should be addressed to S.L.F. (stewart.fisher@astrazeneca.com).